Empirical corrections to the Amber RNA force field with Target Metadynamics

Alejandro Gil-Ley, Sandro Bottaro, and Giovanni Bussi*

Scuola Internazionale Superiore di Studi Avanzati (SISSA), via Bonomea 265, 34136, Trieste, Italy

E-mail: bussi@sissa.it

arXiv:1605.00934v1 [q-bio.BM] 3 May 2016

Abstract

The computational study of conformational transitions in nucleic acids still faces many challenges. For example, in the case of single stranded RNA tetranucleotides, agreement between simulations and experiments is not satisfactory due to inaccuracies in the force fields commonly used in molecular dynamics simulations. We here use experimental data collected from high-resolution X-ray structures to attempt an improvement of the latest version of the AMBER force field. A modified metadynamics algorithm is used to calculate correcting potentials designed to enforce experimental distributions of backbone torsion angles. Replica-exchange simulations of tetranucleotides including these correcting potentials show significantly better agreement with independent solution experiments for the oligonucleotides containing pyrimidine bases. Although the proposed corrections do not seem to be portable to generic RNA systems, the simulations revealed the importance of the α and ζ backbone angles on the modulation of the RNA conformational ensemble. The correction protocol presented here suggests a systematic procedure for force-field refinement.

Introduction

Molecular dynamics is a powerful tool that can be used as a virtual microscope to investigate the structure and dynamics of biomolecular systems.[1] However, the predictive power of molecular dynamics is typically limited by the accuracy of the employed energy functions, known as force fields. Whereas important advances have been made for proteins,[2,3] their accuracy for nucleic acids is still lagging behind.[4,5] Force fields for RNA have been used since several years in many applications to successfully model the dynamics around the experimental structures.[6] Traditionally, the functional form and parameters of these energy functions have been assessed by checking the stability of the native structure. This has lead for instance to the discovery of important flaws in the parametrization of the backbone[7] and of the glycosidic torsion.[8] However, to properly validate a force field it is necessary to ensure that the entire ensemble is consistent with the available experimental data. This can be done only using enhanced sampling techniques or dedicated hardware. Recent tests[5,9] have shown that state-of-the-art force fields for RNA are still not accurate enough to produce ensembles compatible with NMR data in solution in the case of single stranded oligonucleotides. Similar issues have been reported for DNA and RNA dinucleosides.[10,11]

Previous studies have shown that the distribution of structures sampled from the protein data bank (PDB) may approximate the Boltzmann distribution to a reasonable extent[2,12–14] and could even highlight features in the conformational landscape that are not reproduced by state-of-the-art force fields.[15,16] This has been exploited in the

parametrization of protein force fields. For example, a significant improvement of the force fields of the CHARMM family has been obtained by including empirical corrections commonly known as CMAPs based on distributions from the PDB.[17,18]

In this work, we apply these ideas to the RNA field and show how it is possible to derive force-field corrections using an ensemble of X-ray structures. At variance with the CMAP approach, we here correct the force field using a self-consistent procedure where metadynamics is used to enforce a given target distribution.[19,20] Correcting potentials are obtained for multiple dihedral angles using the metadynamics algorithm in a concurrent fashion. Since the target distributions are multimodal, we also use a recently developed enhanced sampling technique, replica exchange with collective-variable tempering (RECT),[21] to accelerate the convergence of the algorithm. The correcting potentials are obtained by matching the torsion distributions for a set of dinucleoside monophosphates. The resulting corrections are then tested on tetranucleotides where standard force field parameters are known to fail in reproducing NMR data.

Methods

In this Section we briefly describe the target metadynamics approach and discuss the details of the performed simulations.

Targeting Distributions with Metadynamics

Metadynamics (MetaD) has been traditionally used to enforce an uniform distribution for a properly chosen set of collective variables (CV) that are expected to describe the slow dynamics of a system.[22] However, it has been recently shown that the algorithm can be modified so as to target a preassigned distribution which is not uniform.[19,20] In this way a distribution taken from experiments, such as pulsed electron paramagnetic resonance, or from an X-ray ensemble, can be enforced to improve the agreement of simulations with empirical data. We refer to the method as target metadynamics (T-MetaD), following the name introduced in ref[19]. For completeness, we here briefly derive the equations. It is also important to notice that the same goal could be achieved using a recently proposed variational approach.[23,24]

In our implementation of T-MetaD a history dependent potential $V(s,t)$ acting on the collective variable s at time t is introduced and evolved according to the following equation of motion

$$\dot{V}(s,t) = \omega e^{\beta(\tilde{F}(s(t))-\tilde{F}_{\max})} e^{-\beta(\frac{V_{\max}}{D})} e^{-\frac{(s-s(t))^2}{2\sigma^2}} \quad (1)$$

Here $\beta = 1/k_B T$, k_B is the Boltzmann constant, T the temperature, ω is the initial deposition rate of the kernel function which is here defined as a Gaussian with width σ, $\tilde{F}$(s) is the free energy landscape associated to the target distribution, $\tilde{F}_{\max}$ indicates the maximum value of the function $\tilde{F}$, and D is a constant damping factor. The target distribution is thus proportional to $e^{-\beta\tilde{F}(s)}$. We define $\omega = \frac{Dk_BT}{\tau}$ where τ is the characteristic time of bias deposition. The term $e^{\beta(\tilde{F}(s)-\tilde{F}_{\max})}$ adjusts the height of the bias potential, making Gaussians higher at the target free-energy maximum and lower at its minimum. This forces the system to spend more time on regions where the targeted free-energy is lower. We notice that a similar argument has been used in the past to derive the stationary distribution of both well-tempered metadynamics, where Gaussian height depends on already deposited potential,[25] and of adaptive-Gaussian metadynamics, where Gaussian shape and volume is changed during the simulation.[26] The subtraction of $\tilde{F}_{\max}$ sets an intrinsic upper limit for the height of each Gaussian, thus avoiding the addition of large forces on the system. We notice that other authors used terms such as the minimum of F or the partition function to set an intrinsic lower limit for the prefactor $e^{\beta(\tilde{F}(s)-\tilde{F}_{\max})}$.[19,20] At the same time, the term $e^{-\beta(\frac{V_{\max}}{D})}$ acts as a global tempering factor[27] and makes the Gaussian height decrease with the simulation time so as to make the bias potential converge instead of fluctuating. As observed in ref[19], the tempering approach used in well-tempered MetaD in this case would lead to a final distribution that is a mixture of the target one with the one from the original force field. For this reason, we prefer to use here a

global tempering approach.[27]

In the long time limit (quasi-stationary condition) the bias potential will on average grow as[25,27]

$$\left\langle \dot{V}(s) \right\rangle = \int ds' \omega e^{\beta(\tilde{F}(s')-\tilde{F}_{\max})} e^{-\beta(\frac{V_{\max}}{D})} e^{-\frac{(s'-s)^2}{2\sigma^2}} P(s') \quad (2)$$

where $P(s)$ is the probability distribution of the biased ensemble. Defining the function $g(s') = \omega e^{\beta(\tilde{F}(s')-\tilde{F}_{\max})} e^{-\beta(\frac{V_{\max}}{D})}$ we can see this equation is a convolution of a Gaussian and a positive definite function.

$$\left\langle \dot{V}(s) \right\rangle = \int ds' e^{-\frac{(s'-s)^2}{2\sigma^2}} g(s') P(s') \quad (3)$$

As shown in ref[25,27] this average should be independent of s in stationary conditions, so that the function $g(s')P(s')$ should be also independent of s', though still dependent on time

$$\omega e^{\beta(\tilde{F}(s(t))-\tilde{F}_{\max})} e^{-\beta(\frac{V_{\max}}{D})} P(s) = C(t) \quad (4)$$

By recognizing that $\tilde{F}_{\max}$ and $V_{\max}$ do not depend on s, one can transform the last equation to

$$e^{\beta \tilde{F}(s)} P(s) = C'(t) \quad (5)$$

which implies that

$$P(s) \propto e^{-\beta \tilde{F}(s)} \quad (6)$$

Thus, the system will sample a stationary distribution of s that is identical to the enforced one.

Whereas the equations are here only described for a single CV, this method can be straightforwardly applied to multiple CVs in a concurrent manner. In this case, the total bias potential is the sum of the one-dimensional bias potentials applied to each degree of freedom. Indeed, similarly to the concurrent metadynamics used in RECT,[21] all the distributions are self-consistently enforced.[20] This is particularly important when biasing backbone torsion angles in nucleic acids since they are highly correlated.[28,29] In this situation it is also convenient to use a biasing method that converges to a stationary potential through a tempering approach, to include in the self-consistent procedure of MetaD an additional effective potential associated to the correlation between the dihedral angles that is as close as possible to convergence.

Simulation Protocols

RNA dinucleoside monophosphates

Fragments of dinucleoside monophosphate with the sequence CC, AA, CA, and AC were extracted from the PDB database of RNA X-ray structures at medium and high resolution (resolution < 3 Å). The selected structures were protonated using *pdb2gmx* tool from GROMACS 4.6.7.[30] Free-energy profiles along the backbone dihedral angles were calculated with the *driver* utility of PLUMED 2.1.[31]

Molecular dynamics simulations of the chosen RNA dinucleoside monophosphate sequences were performed using the Amberff99bsc0$_{\chi OL3}$ force field (named here Amber14).[7,8,32] The systems were solvated in an octahedron box of TIP3P water molecules[33] with a distance between the solute and the box wall of 1 nm. The system charge was neutralized by adding 1 Na^+ counterion. The LINCS[34] algorithm was used to constrain all bonds containing hydrogens and equations of motion were integrated with a timestep of 2 fs. All the systems were coupled to a thermostat through the stochastic velocity rescaling algorithm.[35] For all non-bonded interactions the direct space cutoff was set to 0.8 nm and the electrostatic long-range interactions were treated using the default particle-mesh Ewald[36] settings. An initial equilibration in the NPT ensemble was done for 2 ns, using the Parrinello-Rahman barostat.[37] Production simulations were ran in the NVT ensemble. All the simulations were run using GROMACS 4.6.7[30] patched with a modified version of the PLUMED 2.1 plugin.[31]

T-MetaD simulations were run to enforce the probability distributions of the angles ε_1, ζ_1, α_2 and β_2 (see Fig. 1), which were calculated from the X-ray fragments. The target free-energy profiles were calculated with PLUMED 2.1. Distributions were estimated as combination of Gaussian kernels, with a bandwidth of 0.15 rad, and written on a grid with 200 bins spanning the $(-\pi, \pi)$ range. The bias potential used for the T-MetaD was grown using a characteristic time $\tau = 200$ ps and a dampfactor $D = 100$. Gaussians with a width of 0.15 rad were deposited every $N_G = 500$ steps.

We underline that simulations performed using T-MetaD could be non ergodic for two reasons.

First, there could be significant barriers acting on CVs that are not targeted and thus not biased at this stage (e.g. χ dihedral angles). Second, if the enforced distribution of a CV is bimodal it will be necessary to help the system in exploring both modes with the correct relative probability. It is thus necessary to combine the T-MetaD approach with an independent enhanced-sampling scheme. Here we used RECT, a replica exchange method where a group of CVs is biased concurrently using a different bias factor for each replica and one reference replica is used to accumulate statistics.[21] When T-MetaD and RECT are combined, in each replica a T-MetaD is run with the same settings, including the reference replica. The T-MetaD/RECT simulation was run with 4 replicas for 1 μs each. For each residue the dihedrals of the nucleic acid backbone (α, β, γ, ε, ζ), together with one of the Cartesian coordinates of the ring puckering[38] (Zx) and the glycosidic torsion angle (χ) were chosen as accelerated CVs (see Fig. 1). To help the free rotation of the nucleotide heterocyclic base around the glycosidic bond, the distance between the center of mass of nucleobases was also biased. For the dihedral angles the Gaussian width was set to 0.25 rad and for the distance it was set to 0.05 nm. The Gaussians were deposited every $N_G = 500$ steps. The initial Gaussian height was adjusted to the biasfactor γ of each replica, according to the relation $h = \frac{k_B T(\gamma-1)}{\tau_B} N_G \Delta t$, in order to maintain the same $\tau_B = 12$ ps across the entire replica ladder. The biasfactor γ ladder was chosen in the range from 1 to 2, following a geometric distribution. In replicas with $\gamma \neq 1$ the target free energy was scaled by a factor $1/\gamma$. Exchanges were attempted every 200 steps. Statistic was collected from the unbiased replica. A sample input file is provided as supplementary material (see Fig S1).

Finally, a new RECT simulation was run for each dinucleoside with the bias potentials obtained from the T-MetaD applied statically on each replica. These calculations represent the results obtained with a force field that includes the corrections from the PDB distributions and are thus labeled as Amber$_{pdb}$. Statistics from these simulations were collected to evaluate the effects of the corrections. The simulation time was 1 μs per replica.

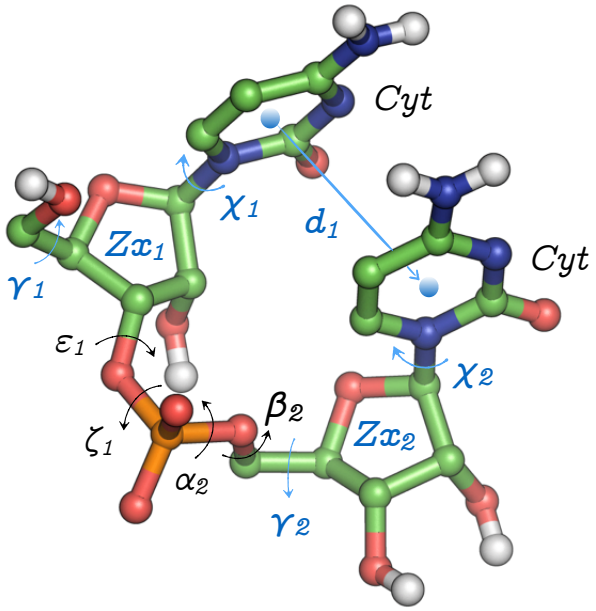

Figure 1: Representation of a Cytosine-Cytosine dinucleoside monophosphate. The backbone dihedrals selected for the force-field correction are shown in black and the CVs accelerated in the RECT simulations are shown in black or blue.

RNA Tetranucleotides

To test the force field corrections derived on dinucleoside monophosphates, temperature replica-exchange molecular dynamics (T-REMD) simulations[39] were performed on different tetranucleotide systems with sequence CCCC, GACC and AAAA. The correcting potentials calculated for the AA and CC dinucleosides were applied to all the backbone angles of AAAA and CCCC tetranucleotides, respectively. For the GACC tetranucleotide we combined the correcting potentials from the T-MetaD simulations of AA, AC and CC, assuming a similarity between purines A and G.

The T-REMD data related to the Amber14 force field and the protocol for the new simulations performed using the Amber$_{pdb}$ force field were taken from ref[16]. The systems were solvated with TIP3P waters and neutral ionic conditions. We used 24 replicas with a geometric distribution of temperatures from 300 to 400 K. Exchanges were attempted every 200 steps. The simulation length was 2.2 μs per replica.

Analysis

The result of the molecular dynamics simulations was compared to NMR experimental data of dinucleosides [10,40–42] and tetranucleotides. [9,43,44] ^3J vicinal coupling constants were calculated using Karplus expressions. [45,46] We took into account the analysis made in refs [10,47,48] to select the most precise sets of parameters. Calculations were performed using the software tool baRNAba[49]. Details are given in the supplementary information, subsection 1.1.

Results

As a first step we used our approach to enforce the dihedral distribution from the X-ray fragments on monophosphate dinucleosides AA, AC, CA, and CC. Then, we show that the corrections are partly transferable and could improve agreement with solution experiments for tetranucleotides.

Calculation of correcting potentials for dinucleoside monophosphates

The Amber14 force field is considered to be one of the most accurate ones for RNA, though it is failing to reproduce solution experiments for short flexible oligomers. Recent benchmarks of different Amber force field modifications based on reparametrization of the torsion angles and nonbonded terms have shown that these changes did not lead to a satisfactory agreement with solution experiments for tetranucleotides. [5,9] On the other hand, ensembles of tetranucleotides taken from the PDB have a very good agreement with NMR data. [16] We thus decided to add correcting potentials to the dihedral angle terms of Amber14, based on information recovered from high-resolution X-ray structures of RNA deposited in the PDB. We analyzed enhanced sampling simulations of dinucleosides (described in this paper) and tetranucleotides (described in a previous publication [16]), to select a minimal amount of degrees of freedom to modify. This analysis indicated the backbone angles ε, ζ, α and β could benefit from a correction (a full description is presented in supplementary information, section 2). We used T-MetaD to enforce on those dihedrals the probability distributions obtained from fragments of X-ray structures. RNA dinucleoside monophosphates were chosen as model systems to obtain the correcting potentials. As the corrections are sequence dependent, for each nucleobase combination we generated an ensemble of experimental conformations from the PDB database that had the same sequence as the dinucleoside monophosphates.

In Fig. 2 we show the free energy profiles of AA and CC dinucleosides projected on the ε, ζ, α and β angles. Amber14, $\text{Amber}_{\text{pdb}}$, as well as the target PDB ensembles are represented. The profiles of AC and CA are shown in Fig S7. The similarity between the PDB and $\text{Amber}_{\text{pdb}}$ profiles makes it clear that the corrections efficiently enforce the distributions taken from the X-ray ensemble. Although some differences are visible around the free-energy barriers, they are expected not to be relevant for room temperature properties at equilibrium. Nevertheless, the transition times and the behavior of the $\text{Amber}_{\text{pdb}}$ potential at high temperatures could be affected by these barriers. In general, barriers in the experimental ensemble are several k_bT lower than those from the Amber14 force field. In the corrected ensemble the multimodal character of the force field probability distributions for the angles ε, ζ and α is reduced, to favor the conformations corresponding to the canonical A-form. The observed agreement between the PDB and $\text{Amber}_{\text{pdb}}$ one-dimensional probability distributions for the selected angles is not necessarily translated into equivalence of the respective ensembles. This is seen for example in the two-dimensional distributions shown in Figs S8-11.

Correcting potentials might in principle also affect the distribution of non-biased degrees of freedom if the latter ones are correlated with the former ones. The distribution of non-biased degrees of freedom, such as the angles γ, χ and puckering coordinate Z_x, is shown in Fig. S12. Overall, no difference is observed between the Amber14 and $\text{Amber}_{\text{pdb}}$ free-energy profiles, with the exception of the ratio between the C3'-*endo* and C2'-*endo* conformations in CC. This is a consequence of the

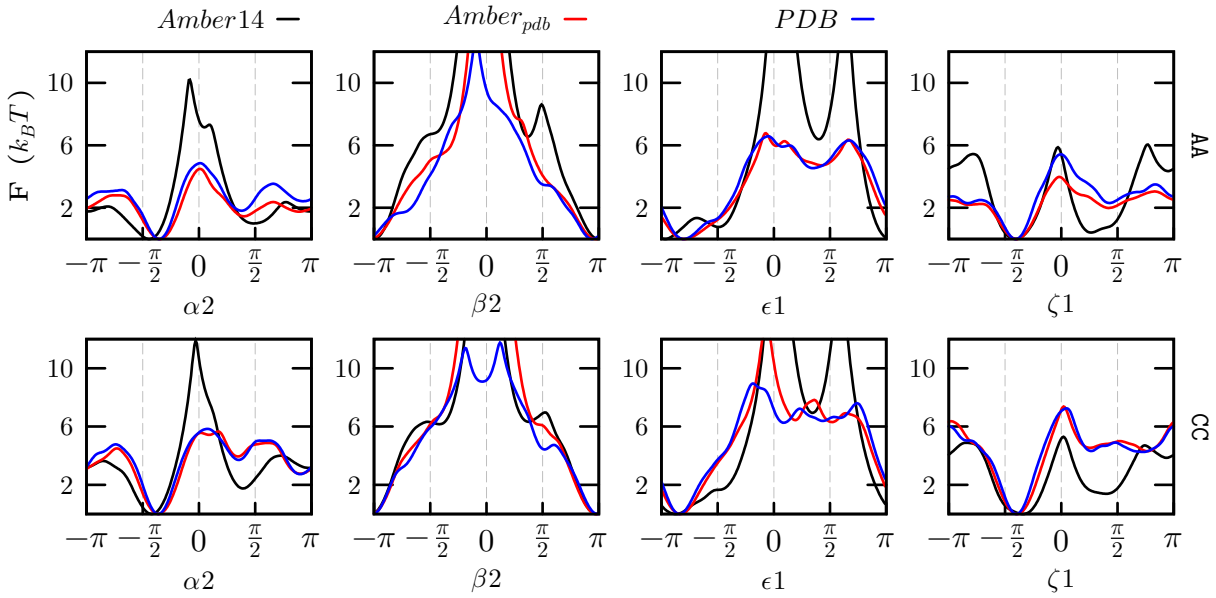

Figure 2: Free-energy profiles of backbone dihedral angles for the AA and CC dinucleosides monophosphates from the X-ray ensemble (PDB) and the RECT simulations with the standard force-field (Amber14) and the correcting potential ($\text{Amber}_{\text{pdb}}$).

significant correlation between the backbone angle ε and the puckering.

To asses the validity of the corrections, we compared all the ensembles against NMR experimental data[10] (Fig 3). Individual ^3J vicinal coupling values from the experiments and the simulations are reported in Table S2. In the case of AA, AC and CA dinucleosides the agreement of $\text{Amber}_{\text{pdb}}$ with the experimental data is better than that of Amber14 and of the X-ray ensemble. This can be explained noticing that $\text{Amber}_{\text{pdb}}$ combines the good agreement with NMR experiments of Amber14 for angles in the nucleoside (dihedrals γ, ν_3 and χ) with that of the PDB distribution for angles in the backbone (dihedrals ε and β), as shown in Fig S13. A notable exception is the CC dinucleoside, where the correlation of backbone angles with puckering mentioned above leads to slightly larger deviation in $\text{Amber}_{\text{pdb}}$ with respect to Amber14. It should be noticed that the NMR observables analyzed here cannot be used to directly determine the conformation around the phosphodiester backbone (α/ζ), so the comparison with the NMR ^3J vicinal coupling dataset does not take into account the distribution of these angles.

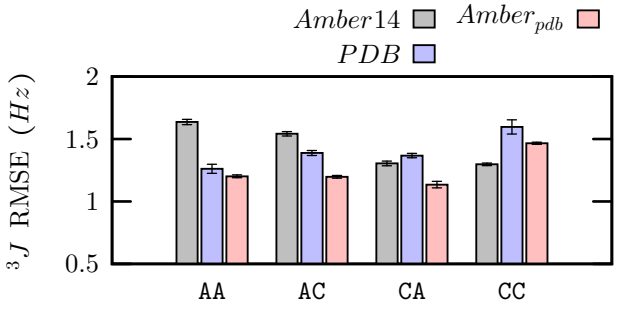

Figure 3: Agreement with the NMR ^3J vicinal coupling dataset of dinucleosides, measured using the root mean square error (RMSE), for the ensembles of X-ray structures (PDB), the Amber force field (Amber14) and the corrected Amber force field ($\text{Amber}_{\text{pdb}}$). Statistical errors were calculated using block averaging.

We noticed that, whereas the NMR data was measured at 293 K (AA, CA and AC) and 320 K (CC), simulations were performed at 300 K. However, the agreement between the data for CC obtained at 320K and similar NMR data obtained for a smaller number of couplings at 280K[42] shows that deviations induced by temperature changes are expected to be much smaller than the typical deviations between molecular dynamics and experiment observed here. It is also important to mention that these RMSE values do not take into

account systematic errors in the Karplus formulas employed in this study.

It is also interesting to measure the effect of the proposed backbone corrections on the stacking interactions. Stacking free energies computed according to the definition used in a recent paper[9] show that the correcting potential have barely no effect on stacking (Fig S14). These numbers can also be compared with experimental values,[41,42,50] and indicate that Amber force field is likely overestimating stacking interactions as suggested by several authors.[51,52] This comparison is however affected by the definition of stacked conformation, which introduces a large arbitrariness in the estimation of stacking free energies from MD.

Validation of Amber$_{pdb}$ potential on RNA tetranucleotides

The correcting potentials discussed above are designed so as to enforce the PDB distribution on dinucleosides monophosphates. We here used these corrections to perform simulations on larger oligonucleotides. In particular, we performed extensive simulations of tetranucleotides, which are considered as good benchmarks for force-field testing, as their small size makes the generation of converged ensembles accessible to modern enhanced sampling techniques. We performed three T-REMD simulations with the Amber$_{pdb}$ potential for the tetranucleotide sequences AAAA, GACC and CCCC. These systems have been used before in very long (hundred of μs) simulations[5,53–56] and NMR experimental data is available.[9,43,44] The Amber14 T-REMD data were taken from ref[16].

The ^3J coupling RMSE, the NOE-distance RMSE, and the number of distance false positives, i.e. the MD predicted NOEs not observed in the experiment, are presented in Fig 4. For these systems the number of false positives is one of the most important parameters to assess the quality of the MD ensembles.[9] In the case of tetranucleotides containing pyrimidines (GACC

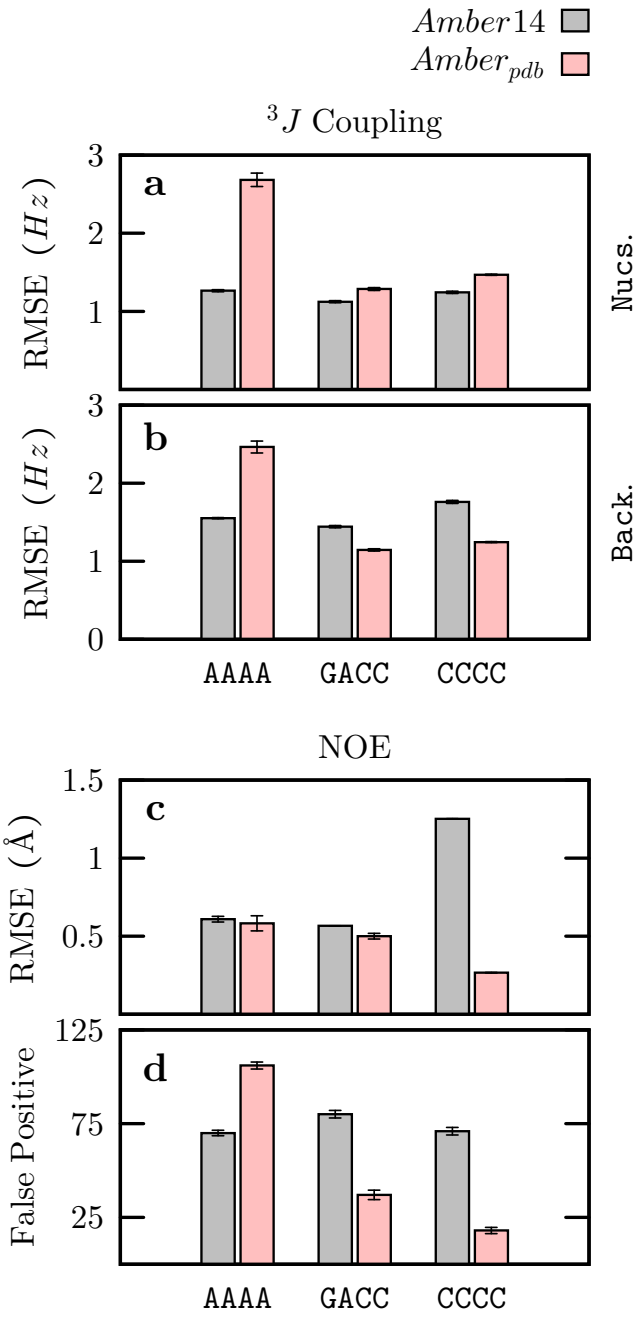

Figure 4: Agreement with the experimental ^3J vicinal couplings and NOE distances of tetranucleotides. For the calculation of the ^3J RMSE the RNA torsion angles were divided in two groups: **a**) the dihedral angles in the ribose-ring region (χ, ν and γ) and **b**) the phosphate-backbone angles (ε, ζ, α and β). In c) the RMSE between calculated and predicted average NOE distances is presented and in **d**) it is shown the number of false positives, i.e. the predicted distances below 5 not observed in the experimental data.

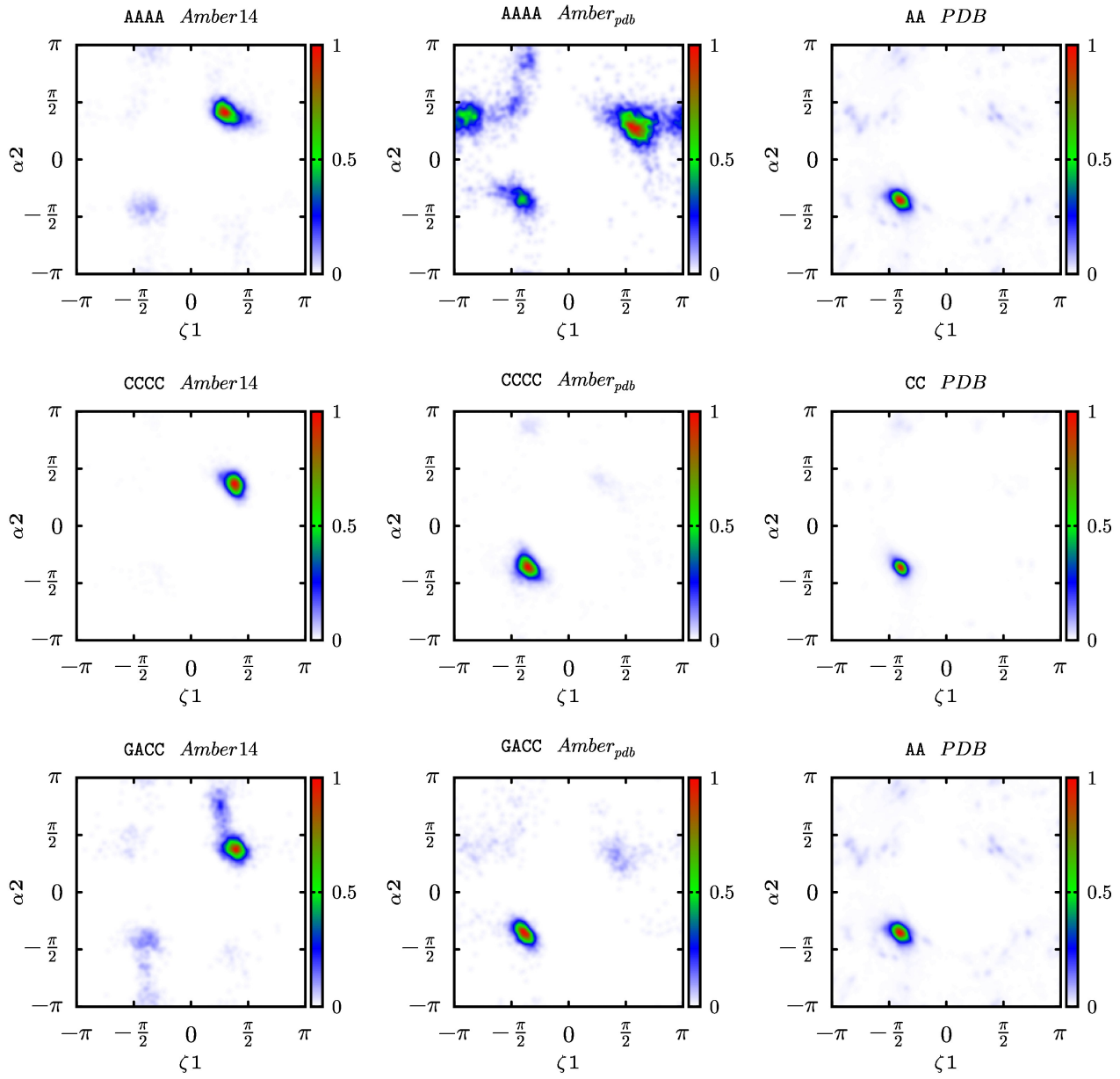

Figure 5: Probability distributions of the backbone dihedral angles of AAAA and CCCC tetranucleotides, in the region between residue 1 and 2. Results from the RECT simulations with the standard force-field (Amber14), the correcting potential (Amber$_{pdb}$) and the dinucleoside X-ray ensembles (PDB) used to generate the correcting potentials.

and CCCC), the correcting potential improves significantly the agreement with the experimental data, mostly for the NOEs (see Fig S15). This is confirmed by the root-mean-square deviation (RMSD) distribution shown in Figure S16 where it can be appreciated that for these two sequences the corrections lead to an overall improvement of the ensemble by disfavoring the intercalated and inverted structures with a large RMSD from native. A completely different scenario is found for the Amber$_{pdb}$ ensemble of AAAA, where the corrections surprisingly diminish the agreement with experiments. This can be also appreciated in a shift of the Amber$_{pdb}$ RMSD distribution peaks to higher RMSD values due to an increase in the population of compact structures (Fig S16). It should be noticed that the effect of the correcting potentials in purines and pyrimidines depends

strongly on the sequence length. Whereas the AAAA tetranucleotide is negatively affected by the corrections, the AA dinucleoside is the one that benefits the most from them.

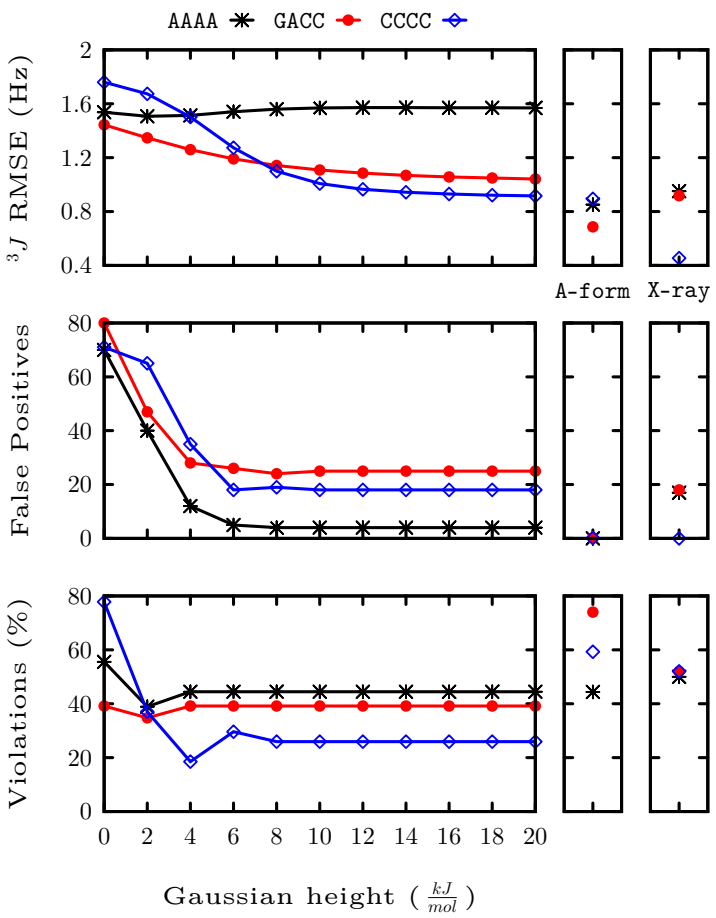

Figure 6: Agreement with the experimental data for the Amber14 reweighted ensemble as a function of the Gaussian potential height. The bias potential was centered on $\alpha(g+)/\zeta(g+)$ conformation $(\frac{\pi}{2}, \frac{\pi}{2})$ with a sigma per angle of 0.7 rad. "A-form" represent a canonical A-form structure and "X-ray" an ensemble of tetranucleotide fragments, with the same sequence, from the PDB (all taken from ref[16]).

As discussed in the section 2 of the SI, the conformation along the phosphodiester backbone is very different between compact and extended tetranucleotide structures. The probability distribution maps of the α_2/ζ_1 backbone dihedral angles from the tetranucleotides T-REMD simulations and the dinucleosides X-ray ensembles used to generate the corrections are depicted in Fig 5. Only phosphodiester backbone torsion angles are shown, because they are the ones mostly affected by the correction. The other backbone angles maps are shown in the SI (Figs S17-25). In the PDB ensembles the distributions are always unimodal, independently of the sequence, with a peak at the $\alpha(g-)/\zeta(g-)$ conformation, whereas in the Amber14 ensemble the $\alpha(g+)/\zeta(g+)$ and $\alpha(g-)/\zeta(g-)$ conformations are both significantly populated. The effects of the corrections, as seen before, are highly sequence dependent. In case of GACC and CCCC, the $\alpha(g-)/\zeta(g-)$ rotamer is stabilized in the $\text{Amber}_{\text{pdb}}$ distributions, with the population of $\alpha(g+)/\zeta(g+)$ significantly decreased with respect to Amber14. On the contrary, for AAAA the $\alpha(g+)/\zeta(g+)$ conformation is not unfavored by the correcting potentials, despite not being significantly present in the PDB ensemble. This could be due to the fact that the one dimensional target free-energy profile for dihedrals α and ζ for the AA (Fig 2) exhibits barriers which are approximately 4 k_bT smaller with respect to the ones from the Amber14 force field. The effect of the decreased barrier height can be appreciated in the α_2/ζ_1 probability distribution of AAAA, where the amount of torsional space explored is increased by the corrections.

Consequences on future force field refinements

The good agreement of the $\text{Amber}_{\text{pdb}}$ ensembles with the NMR observables, in the case of CCCC and GACC tetranucleotides, suggests that the RNA conformational space sampled by state-of-the-art force field could be modified to better match experimental solution data by penalizing rotamers of the α and ζ angles. As a further test, we reweighted the T-REMD Amber14 ensembles with an additional two-dimensional penalizing Gaussian potential centered on the $\alpha(g+)/\zeta(g+)$ conformation. Results are shown in Fig 6 for different Gaussian heights. Overall, the agreement with the NMR experimental data improves considerably with respect to the original force field as the Gaussian height increases. The relative population of the α/ζ conformations has an important impact on the number of false positive NOE contacts which indicates the presence of intercalated

structures. This improvement is achieved without changing the non bonded interactions as it has also been proposed.[51] It is however important to observe that these results are obtained by performing a reweighting, and that corrections should be validated by performing separate simulations with this bias potential.

Discussion

In this paper we apply targeted metadynamics to sample preassigned distributions taken from experimental data.[19,20] At variance with the original applications, we here combine T-MetaD with enhanced sampling showing that these protocols can also be used when the investigated ensembles have non-trivial energy landscapes separated by significant barriers .

We apply the method to RNA oligonucleotides, for which the Amber14 force field was proven to be in significant disagreement with solution NMR data.[5,9,43,44,53,54,56,57] Since tetranucleotide fragments extracted from high resolution structures in the PDB were shown to match NMR experiments better than Amber14 force field,[16] we here used X-ray structures to build reference distributions of backbone dihedral angles that are then used to devise correcting potentials. More precisely, we use T-MetaD to enforce the empirical distribution of the dihedral angles in the phosphate backbone (ε, α, ζ and β) on four dinucleoside monophosphates.

We calculated the correcting potentials concurrently for all the four angles in order to change the distribution of these consecutive dihedrals along the backbone chain taking into account their correlation. The method successfully enforced the distributions taken from the PDB on all the angles. The new ensemble generated by the corrected force field ($\text{Amber}_{\text{pdb}}$) was independently validated against solution NMR data that was not used in the fitting of the corrections. For three of the four dinucleosides studied, $\text{Amber}_{\text{pdb}}$ showed a better agreement with the NMR data compared with Amber14 and with the X-ray ensemble.

We then tested the portability of the correcting potentials by simulating three tetranucleotides, GACC, CCCC and AAAA. In the case of GACC and CCCC the agreement with NMR data is significantly improved by the corrections. Surprisingly, for AAAA the corrections have the opposite effect and increase the probability of visiting compact structures making the simulated ensemble less compatible with solution experiments. It should be noticed here that this is a non obvious result since the PDB database is expected to have an intrinsic bias towards A-form structures and should thus in principle increase the agreement with solution experiments in this specific case. This indicates that porting the corrections from dinucleosides to tetranucleotides is not straightforward because the coupling between the multiple corrected dihedrals could affect the resulting ensemble in an non-trivial way. Additionally, corrections applied to dihedral angles alone might be not sufficient to compensate errors arising from inexact parametrization of van der Waals or electrostatic interactions.[51] Overall, the tests we performed indicate that the corrections derived here should not be considered as portable corrections for the simulation of generic RNA sequences.

Nevertheless, by comparing the backbone angle distributions on the different RNA simulations and the X-ray ensembles, we were able to find possible hints pointing at where refinement of dihedral potentials could lead to an advancement in RNA force fields. In this respect, the results for GACC an CCCC show the significant improvement observed in the $\text{Amber}_{\text{pdb}}$ simulations for those systems could be reproduced by simply penalizing the $\alpha(g+)/\zeta(g+)$ conformation, which is overpopulated in Amber14. By a straightforward reweighting procedure, we showed that simple Gaussian potentials that disfavor this conformation significantly improved the experimental agreement with solution experiments for all the three tetranucleotides. Recent modifications of the Lennard-Jones parameters for phosphate oxygens[58] and different water models[56] were shown to affect the conformational ensemble of RNA tetranucleotides.[5,56] It might be interesting to combine these modified parameters for nonbonded interactions with the here introduced procedure for dihedral angle refinement.

The nature of the correction methodology discussed in this paper is very different from the classical approach to force field parametrization,

as it aims to correct the free energy of the system, instead of fitting the potential energy landscape of the dihedral angles while constraining the other degrees of freedom. It is important to notice that the dihedral angle distributions taken from the fragments of the PDB structures do not necessarily represent the conformational ensembles of dinucleosides or tetranucleotides in solution. Indeed, some of the interaction patterns that are present in large structures crystallized in the PDB do not exist in short oligonucleotides. For this reason, in this work the distributions were validated against independent solutions NMR experiments. This allowed the dihedral angles from the PDB distributions that performed better than the force field to be identified. We also recall that in our procedure the force-field torsion energy function is not refitted, but a bias potential is added to the total energy of the system in order to match the free-energy profile of the torsion angles with target ones. Thus, a major advantage of this approach is that it takes explicitly into account the entropic contributions, the cross correlations between torsional angles, and inaccuracies in the non-bonded interactions, among other effects.

Conclusion

In conclusion, in this work we applied the target metadynamics protocol to modify dihedral distributions in dinucleosides. The procedure successfully enforces reference distributions taken from the PDB without affecting the distribution of the dihedral angles that were not biased. However, the attempt to port these corrections to tetranucleotides lead to ambiguous results when applied to different sequences. This could be partly due to the fact that distribution form the PDB are not necessarily a good reference for refinement.

Nevertheless, the simulations revealed the importance of the α/ζ angles rotamers on the modulation of the conformational ensemble, and that by only penalizing the $\alpha(g+)/\zeta(g+)$ rotamer the quality of the ensemble is significantly improved to levels not reported before.

Acknowledgement

Thomas Cheatham III, Fabrizio Marinelli, and Jiří Šponer are acknowledged for carefully reading the manuscript and providing several useful suggestions. The research leading to these results has received funding from the European Research Council under the European Union's Seventh Framework Programme (FP/2007-2013) / ERC Grant Agreement n. 306662, S-RNA-S.

References

(1) Dror, R. O.; Dirks, R. M.; Grossman, J.; Xu, H.; Shaw, D. E. *Annu. Rev. Biophys.* **2012**, *41*, 429–452.

(2) Lindorff-Larsen, K.; Piana, S.; Palmo, K.; Maragakis, P.; Klepeis, J.; Dror, R.; Shaw, D. *Proteins: Struct., Funct., Bioinf.* **2010**, *78*, 1950–1958.

(3) Lindorff-Larsen, K.; Maragakis, P.; Piana, S.; Eastwood, M. P.; Dror, R. O.; Shaw, D. E. *PloS one* **2012**, *7*, e32131.

(4) Šponer, J.; Banáš, P.; Jurecka, P.; Zgarbova, M.; Kührová, P.; Havrila, M.; Krepl, M.; Stadlbauer, P.; Otyepka, M. *J. Phys. Chem. Lett.* **2014**, *5*, 1771–1782.

(5) Bergonzo, C.; Henriksen, N. M.; Roe, D. R.; Cheatham, T. E. *RNA* **2015**, *21*, 1578–1590.

(6) Cheatham, T. E.; Case, D. A. *Biopolymers* **2013**, *99*, 969–977.

(7) Pérez, A.; Marchán, I.; Svozil, D.; Šponer, J.; Cheatham III, T. E.; Laughton, C. A.; Orozco, M. *Biophys. J.* **2007**, *92*, 3817–3829.

(8) Zgarbová, M.; Otyepka, M.; Šponer, J.; Mládek, A.; Banáš, P.; Cheatham III, T. E.; Jurecka, P. *J. Chem. Theory Comput.* **2011**, *7*, 2886–2902.

(9) Condon, D. E.; Kennedy, S. D.; Mort, B. C.; Kierzek, R.; Yildirim, I.; Turner, D. H. *J. Chem. Theory Comput.* **2015**, *11*, 2729–2742.

(10) Vokáčová, Z.; Budesinsky, M.; Rosenberg, I.; Schneider, B.; Šponer, J.; Sychrovský, V. *J. Phys. Chem. B* **2009**, *113*, 1182–1191.

(11) Nganou, C.; Kennedy, S. D.; McCamant, D. W. *J. Phys. Chem. B* **2016**, *120*, 1250–1258.

(12) Butterfoss, G. L.; Hermans, J. *Protein Sci.* **2003**, *12*, 2719–2731.
(13) MacKerell, A. D.; Feig, M.; Brooks, C. L. *J. Comput. Chem.* **2004**, *25*, 1400–1415.
(14) Morozov, A. V.; Kortemme, T.; Tsemekhman, K.; Baker, D. *Proc. Natl. Acad. Sci. U.S.A.* **2004**, *101*, 6946–6951.
(15) Brereton, A. E.; Karplus, P. A. *Sci. Adv.* **2015**, *1*, e1501188.
(16) Bottaro, S.; Gil-Ley, A.; Bussi, G. *Nucleic Acids Res.* **2016**, doi:10.1093/nar/gkw239
(17) MacKerell, A. D.; Feig, M.; Brooks, C. L. *J. Am. Chem. Soc.* **2004**, *126*, 698–699.
(18) Buck, M.; Bouguet-Bonnet, S.; Pastor, R. W.; MacKerell, A. D. *Biophys. J.* **2006**, *90*, L36–L38.
(19) White, A.; Dama, J.; Voth, G. A. *J. Chem. Theory Comput.* **2015**, *11*, 2451–2460.
(20) Marinelli, F.; Faraldo-Gómez, J. D. *Biophys. J.* **2015**, *108*, 2779–2782.
(21) Gil-Ley, A.; Bussi, G. *J. Chem. Theory Comput.* **2015**, *11*, 1077–1085.
(22) Laio, A.; Parrinello, M. *Proc. Natl. Acad. Sci. U. S. A.* **2002**, *99*, 12562–12566.
(23) Valsson, O.; Parrinello, M. *Phys. Rev. Lett.* **2014**, *113*, 090601.
(24) Shaffer, P.; Valsson, O.; Parrinello, M. *Proc. Natl. Acad. Sci. U.S.A.* **2016**, *113*, 1150–1155.
(25) Barducci, A.; Bussi, G.; Parrinello, M. *Phys. Rev. Lett.* **2008**, *100*, 020603.
(26) Branduardi, D.; Bussi, G.; Parrinello, M. *J. Chem. Theory Comput.* **2012**, *8*, 2247–2254.
(27) Dama, J. F.; Parrinello, M.; Voth, G. A. *Phys. Rev. Lett.* **2014**, *112*, 240602.
(28) Saenger, W. *Principles of Nucleic Acid Structure*; Springer-Verlag, New York, 1984.
(29) Richardson, J. S.; Schneider, B.; Murray, L. W.; Kapral, G. J.; Immormino, R. M.; Headd, J. J.; Richardson, D. C.; Ham, D.; Hershkovits, E.; Williams, L. D.; Keating, K. S.; Pyle, A. M.; Micallef, D.; Westbrook, J.; Berman, H. M. *RNA* **2008**, *14*, 465–481.
(30) Hess, B.; Kutzner, C.; Van Der Spoel, D.; Lindahl, E. *J. Chem. Theory Comput.* **2008**, *4*, 435–447.
(31) Tribello, G. A.; Bonomi, M.; Branduardi, D.; Camilloni, C.; Bussi, G. *Comput. Phys. Commun.* **2014**, *185*, 604–613.
(32) Cornell, W. D.; Cieplak, P.; Bayly, C. I.; Gould, I. R.; Merz, K. M.; Ferguson, D. M.; Spellmeyer, D. C.; Fox, T.; Caldwell, J. W.; Kollman, P. A. *J. Am. Chem. Soc.* **1995**, *117*, 5179–5197.
(33) Jorgensen, W. L. *J. Am. Chem. Soc.* **1981**, *103*, 335–340.
(34) Hess, B.; Bekker, H.; Berendsen, H. J.; Fraaije, J. G. *J. Comput. Chem.* **1997**, *18*, 1463–1472.
(35) Bussi, G.; Donadio, D.; Parrinello, M. *J. Chem. Phys.* **2007**, *126*, 014101.
(36) Darden, T.; York, D.; Pedersen, L. *J. Chem. Phys.* **1993**, *98*, 10089–10092.
(37) Parrinello, M.; Rahman, A. *J. Appl. Phys.* **1981**, *52*, 7182–7190.
(38) Huang, M.; Giese, T. J.; Lee, T.-S.; York, D. M. *J. Chem. Theory Comput.* **2014**, *10*, 1538–1545.
(39) Sugita, Y.; Okamoto, Y. *Chem. Phys. Lett.* **1999**, *314*, 141–151.
(40) Olsthoorn, C. S.; Doornbos, J.; Leeuw, H. P.; Altona, C. *Eur. J. Biochem.* **1982**, *125*, 367–382.
(41) Ezra, F. S.; Lee, C.-H.; Kondo, N. S.; Danyluk, S. S.; Sarma, R. H. *Biochemistry* **1977**, *16*, 1977–1987.
(42) Lee, C.-H.; Ezra, F. S.; Kondo, N. S.; Sarma, R. H.; Danyluk, S. S. *Biochemistry* **1976**, *15*, 3627–3639.
(43) Yildirim, I.; Stern, H. A.; Tubbs, J. D.; Kennedy, S. D.; Turner, D. H. *J. Phys. Chem. B* **2011**, *115*, 9261–9270.
(44) Tubbs, J. D.; Condon, D. E.; Kennedy, S. D.; Hauser, M.; Bevilacqua, P. C.; Turner, D. H. *Biochemistry* **2013**, *52*, 996–1010.
(45) Karplus, M. *J. Chem. Phys.* **1959**, *30*, 11–15.
(46) Karplus, M. *J. Am. Chem. Soc.* **1963**, *85*, 2870–2871.
(47) Sychrovskỳ, V.; Vokácová, Z.; Šponer, J.; Špacková, N.; Schneider, B. *J. Phys. Chem. B* **2006**, *110*, 22894–22902.
(48) Vokáčová, Z.; Bickelhaupt, F. M.; Šponer, J.; Sychrovský, V. *J. Phys. Chem. A* **2009**, *113*, 8379–8386.
(49) Bottaro, S.; Di Palma, F.; Bussi, G. *Nucleic Acids Res.* **2014**, *42*, 13306–14.
(50) Frechet, D.; Ehrlich, R.; Remy, P.; Gabarro-

Arpa, J. *Nucleic Acids Res.* **1979**, *7*, 1981–2001.
(51) Chen, A. A.; García, A. E. *Proc. Natl. Acad. Sci. U. S. A.* **2013**, *110*, 16820–16825.
(52) Brown, R. F.; Andrews, C. T.; Elcock, A. H. *J. Chem. Theory Comput.* **2015**, *11*, 2315–2328.
(53) Bergonzo, C.; Henriksen, N. M.; Roe, D. R.; Swails, J. M.; Roitberg, A. E.; Cheatham III, T. E. *J. Chem. Theory Comput.* **2013**, *10*, 492–499.
(54) Henriksen, N. M.; Roe, D. R.; Cheatham III, T. E. *J. Phys. Chem. B* **2013**, *117*, 4014–4027.
(55) Roe, D. R.; Bergonzo, C.; Cheatham III, T. E. *J. Phys. Chem. B* **2014**, *18*, 3543–52.
(56) Bergonzo, C.; III, T. E. C. *J. Chem. Theory Comput.* **2015**, *11*, 3969–3972.
(57) Condon, D. E.; Yildirim, I.; Kennedy, S. D.; Mort, B. C.; Kierzek, R.; Turner, D. H. *J. Phys. Chem. B* **2014**, *118*, 1216–1228.
(58) Steinbrecher, T.; Latzer, J.; Case, D. *J. Chem. Theory Comput.* **2012**, *8*, 4405–4412.